Monthly Notices of the ROYAL ASTRONOMICAL SOCIETY

MNRAS **516,** 5084–5091 (2022) https://doi.org/10.1093/mnras/stac2423
Advance Access publication 2022 August 27

Pulsar death line revisited – II. 'The death valley'

V. S. Beskin[1,2★] and A. Yu. Istomin[2]

[1] *P.N. Lebedev Physical Institute, Leninsky prospect 53, Moscow 119991, Russia*
[2] *Moscow Institute of Physics and Technology, Dolgoprudny, Moscow region, Institutsky per. 9, Moscow 141700, Russia*

Accepted 2022 August 24. Received 2022 August 23; in original form 2022 April 7

ABSTRACT

In this paper, which is the second in a series of papers, we analyse what parameters can determine the width of the radio pulsar 'death valley' in the P–$\dot{P}$ diagram. Using exact expression for the maximum potential drop, which can be realized over magnetic polar caps and the corresponding threshold for the secondary plasma production determined in Paper I, we analyse in detail the observed distribution of pulsars taking into account all the possible parameters (radius R and moment of inertia of a neutron star $I_{\rm r}$, high-energy tail in the γ-quanta energy distribution giving rise to secondary particles, etc.) which could broaden 'the death line'. We show that the consistent allowance for all these effects leads to a sufficiently wide of 'the death valley' containing all the observed pulsars even for dipole magnetic field of a neutron star. We emphasize that the main goal of this work is to demonstrate that the original Ruderman–Sutherland idea of the death line (dipole magnetic field, vacuum gap) is in good agreement with observations. The comparison with other models is beyond the scope of this paper.

Key words: stars: neutron – pulsars: general.

1 INTRODUCTION

Pulsar radio emission is believed to be produced by a secondary electron–positron plasma generated in the polar regions of a neutron star (Sturrock 1971; Ruderman & Sutherland 1975; Arons 1982; Lorimer & Kramer 2012; Lyne & Graham-Smith 2012). For this reason, the cessation condition for the generation of secondary particles is associated with the so-called 'death line' on the P–$\dot{P}$ diagram, where P is the pulsar period, and $\dot{P}$ is its time derivative. However, despite in-depth research on the generation of secondary plasma conducted since the beginning of the eighties of the last century (Daugherty & Harding 1982; Gurevich & Istomin 1985; Arendt & Eilek 2002; Istomin & Sobyanin 2007; Medin & Lai 2010; Timokhin 2010; Timokhin & Arons 2013; Philippov, Spitkovsky & Cerutti 2015; Timokhin & Harding 2015; Cerutti, Philippov & Spitkovsky 2016) up to now, a large number of different options have been discussed in the literature (Ruderman & Sutherland 1975; Blandford & Scharlemann 1976; Arons 1982; Usov & Melrose 1995), leading to markedly different conditions which set 'the death line' of radio pulsars (Chen & Ruderman 1993; Zhang, Harding & Muslimov 2000; Hibschman & Arons 2001; Faucher-Giguére & Kaspi 2006; Konar & Deka 2019).

We immediately note that in this series of works, we discuss the 'classical' mechanism of particle production only. As is well-known, this process includes primary particle acceleration by a longitudinal electric field, γ-quanta emission due to curvature radiation, production of secondary electron–positron pairs, and, finally, secondary particles acceleration in the opposite direction, which also leads to the creation of secondary particles (Sturrock 1971; Ruderman & Sutherland 1975). Thus, we do not consider particle production due to Inverse Compton Scattering, which, as is well-known (Blandford & Scharlemann 1976; Zhang et al. 2000; Barsukov, Kantor & Tsygan 2007), can also be a source of hard γ-quanta. As an excuse, we note that first of all, we will be interested in old pulsars, in which the surface temperature may not be high enough to form a sufficient number of X-ray photons.

Moreover, we also do not include into consideration synchrotron photons emitted by secondary pairs. The point is that the energy of synchrotron photons emitted by secondary particles is approximately 15–20 times less than the energy of curvature photons emitted by primary particles (see e.g. Gurevich & Istomin 1985; Istomin & Sobyanin 2007). Therefore, near the threshold for particle production, when the free path lengths of curvature photons becomes close to the radius of the star R, the pulsar magnetosphere turns out to be transparent for synchrotron photons.

As a result, as was first shown by Ruderman & Sutherland (1975), the cessation condition for the pair creation determining the position of 'the death line' on the P–$\dot{P}$ diagram can be evaluated from the equality of the height of the 1D vacuum gap

$$H_{\rm RS} \sim \left(\frac{\hbar}{m_{\rm e}c}\right)^{2/7} \left(\frac{B_0}{B_{\rm cr}}\right)^{-4/7} R_{\rm L}^{3/7} R_{\rm c}^{2/7} \qquad (1)$$

and the polar cap radius

$$R_{\rm cap} \approx \left(\frac{\Omega R}{c}\right)^{1/2} R. \qquad (2)$$

Here, $B_{\rm cr} = m_{\rm e}^2 c^3/e\hbar = 4.4 \times 10^{13}$ G is the Schwinger magnetic field, $R_{\rm L} = c/\Omega$ is the radius of the light cylinder ($\Omega = 2\pi/P$ is the star angular velocity), and $R_{\rm c}$ is the curvature of magnetic field lines near the magnetic pole. For magneto-dipole energy losses

$$W_{\rm tot} \sim \frac{B_0^2 \Omega^4 R^6}{c^3} \qquad (3)$$

★ E-mail: beskin@lpi.ru

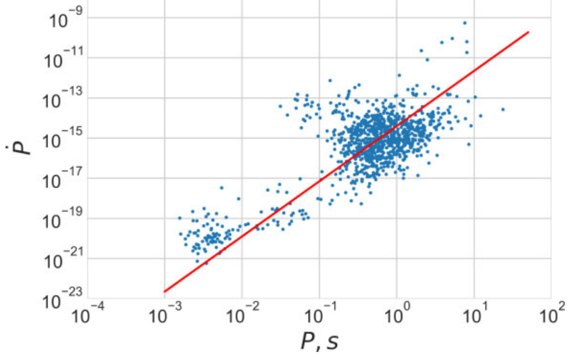

Figure 1. P–$\dot{P}$ diagram taken from the ATNF catalogue (Manchester et al. 2005). The line corresponds to relation (5) with $\beta_{\rm d} = 4$ obtained by Chen & Ruderman (1993) for dipole magnetic field.

and the dipole magnetic field stricture, when

$$R_{\rm c} = \frac{4}{3}\frac{r}{\theta_m}, \tag{4}$$

(r and θ_m are the polar coordinates relative to the magnetic axis, r is the distance from the star centre), one can obtain for 'the death line' (Ruderman & Sutherland 1975)

$$\dot{P}_{-15} = \beta_{\rm d} P^{11/4}, \tag{5}$$

where $\dot{P}_{-15} = 10^{15}\dot{P}$ and $\beta_{\rm b}^{\rm RS} \sim 1$.

It is clear that in the mid-70s such accuracy was quite acceptable, especially since expression (5) really limited from below most of the pulsars in the P–$\dot{P}$ diagram. However, as was already noted, at present this issue requires substantial revision. Indeed, as one can see form Fig. 1, there are many radio pulsars below 'the death line' drawn for characteristic values, i.e. for neutron star radius $R =$ 10 km and magnetic field $B_0 = 10^{12}$ G ($\beta_{\rm d} = 4$ according to Chen & Ruderman 1993). As can be seen from Table 1, the derivative of the period for some pulsars turns out to be 1–2 orders of magnitude less than that of the classical Ruderman–Sutherland death line, i.e. gives: $\beta_{\rm d} = (0.01$–$0.1)\beta_{\rm d}^{\rm RS}$.

On the other hand, it is important that their number decreases with the distance from it. In total, there are 110 pulsars with $\beta_{\rm d} < 0.1$, and only 21 pulsar with $\beta_{\rm d} < 0.02$. This implies that in reality we deal with 'the death valley' corresponding to the tail of the distribution with respect to some parameters. Therefore, one of the main tasks of our consideration is the question of which parameter leads to a decrease in the observed deceleration rate $\dot{P}$.

The idea of 'the death valley' is not new. It was first discussed by Chen & Ruderman (1993), who introduced this term, and then this issue was discussed in many other works (see e.g. Zhang et al. 2000; Gonthier et al. 2002; Kou & Tong 2015). In particular, the authors discussed a possible role of a non-dipole magnetic field. However, none of these works, based on qualitative estimates, studied quantitatively the question of the real 3D structure of the particle acceleration region, not to say about the spread of such parameters as the masses and moments of inertia of neutron stars.

To clarify this issue, in Paper I (Beskin & Litvinov 2022), we set ourselves a task to reconsider all the basic approximations which are usually used in constructing of the model the secondary plasma generation, but which may work poorly near 'the death line'. These refinements concerned the electric potential, the influence of the emission spectrum of primary particles, and the effects of general relativity. Such a detailed study has never been done before.

As a result, the conditions for the cascade generation of particles were formulated, which we will consider here as a condition which determines 'the death line' on the P–$\dot{P}$ diagram. Let us emphasize that as both relativistic corrections and the connection between the deceleration rate $\dot{P}$ and the magnetic field depend on the radius R and moment of inertia $I_{\rm r}$, we, in fact, deal with a rather wide 'death valley', i.e. with a sufficiently wide area whose width depends on the spread of these values. Determining the real width of 'the death valley', as well as explaining the existence of radio pulsars with extremely low deceleration rates is the main goal of this work.

We emphasize once again that the main goal of this work was to demonstrate that the original Ruderman–Sutherland idea of the death line (dipole magnetic field, vacuum gap) leading to dependence (5) is in good agreement with observations. In other words, we show below that the agreement is achieved even within the framework of the power dependence $\dot{P} \propto P^{11/4}$, since the simultaneous taking into account all the effects mentioned above reduces significantly the coefficient $\beta_{\rm b}$. Thus, comparison with other models is beyond the scope of this article.

For this reason, in this paper we consider only a dipole magnetic field, despite a large number of works which indicated that it is impossible to explain 'the death line' in a dipole magnetic field (Arons 1993; Asseo & Khechinashvili 2002; Barsukov & Tsygan 2010; Igoshev, Elfritz & Popov 2016; Bilous et al. 2019). In particular, we do not discuss the model with a fixed curvature radius $R_{\rm c} = R$, also considered by Chen & Ruderman (1993). By the way, taking into account the effects discussed in Paper I this boundary (it corresponds to dependence $\dot{P} \propto P^2$) should be located well below the observed pulsars.

As an additional argument, we can cite a sufficiently large number of pulsars with drifting subpulses (Weltevrede, Edwards & Stappers 2006; Weltevrede, Stappers & Edwards 2007), for which, in the framework of the carousel model (van Leeuwen et al. 2003; Janssen & van Leeuwen 2004; Mitra & Rankin 2008), a regular axisymmetric magnetic field is required. Moreover, it is precisely in the region of plasma generation, since it is this region that determines the drift velocity. Such a configuration is hardly possible for a random orientation of the nondipole component. Of course, individual pulsars can have a significant non-dipole magnetic field (for example, as a pulsar PSR J0030 + 0451, see Riley et al. 2019 for more detail).

Finally, another important argument is that the original idea of a vacuum gap, which underlies the Ruderman–Sutherland model, has recently been unexpectedly confirmed. As shown by Timokhin & Arons (2013), due to the strong non-stationarity of the process of particle production, a vacuum region actually appears from time to time. In this case, the heights of the vacuum gap determining the particle creation rate practically coincides with the Ruderman–Sutherland estimate (1).

The paper is organized as follows. In Section 2, we present a summary of the main results obtained in Paper I. They refer to all possible amendments which have not yet been taken into account together. In addition, the parameters of two evolutionary scenarios are formulated in what follows. Further, in Section 3, the real boundaries of 'the death valley' are determined, which are in good agreement with the observations. Then, after discussing the nature of the knee in 'the death line' in Section 4, a discussion of the results is given in Section 5.

2 BASIC EQUATIONS

2.1 Paper I – general results

At first, in Paper I, we assumed that due to time irregularity of the secondary plasma production (Timokhin 2010; Timokhin & Arons

Table 1. Pulsars deep below 'the death line' ($\beta_{\rm d} < 0.02$) taken from the ATNF catalogue (Manchester et al. 2005). See the text for more detail.

PSR	P (s)	$\dot{P}_{-15}$	$B_{12}^{\rm ATNF}$	$B_{12}^{\rm MHD}$ ($\chi = 60^\circ$)	$B_{12}^{\rm BGI}$ ($\chi = 60^\circ$)	Λ	$\mathcal{K}$	ξ	$\beta_{\rm d}$
J0250 + 5854	23.53	27.16	25.66	25.88	42.80	39	1.5×10^5	7.1	0.003
J0343 − 3000	2.60	0.06	0.39	0.39	0.65	37	1.1×10^6	8.6	0.004
J0418 + 5732	9.01	4.10	6.17	6.22	10.29	35	7.3×10^4	6.6	0.010
J0457 − 6337	2.50	0.21	0.74	0.74	1.23	33	1.3×10^5	7.1	0.017
J0656 − 2228	1.23	0.03	0.18	0.19	0.31	33	3.5×10^5	7.8	0.015
J0901 − 4046	75.89	215.	128	129	214	42	1.2×10^5	7.9	0.001
J0919 − 6040	1.22	0.01	0.11	0.11	0.19	36	1.5×10^6	8.9	0.006
J1210 − 6550	4.24	0.43	1.37	1.38	2.29	35	2.2×10^5	7.3	0.008
J1232 − 4742	1.87	0.01	0.16	0.17	0.27	39	3.3×10^6	9.4	0.003
J1320 − 3512	0.46	0.002	0.03	0.03	0.05	32	9.0×10^5	8.4	0.017
J1333 − 4449	0.46	0.0005	0.01	0.01	0.02	34	3.2×10^6	9.4	0.009
J1503 + 2111	3.32	0.14	0.69	0.71	1.15	37	5.8×10^5	8.1	0.005
J1638 − 4344	1.12	0.02	0.17	0.17	0.28	32	2.9×10^5	7.6	0.018
J1801 − 1855	2.55	0.18	0.69	0.69	1.15	33	1.8×10^5	7.3	0.014
J1805 − 2447	0.66	0.006	0.06	0.06	0.11	32	5.1×10^5	8.0	0.019
J1859 + 7654	1.39	0.05	0.27	0.27	0.45	32	2.0×10^5	7.4	0.020
J1915 + 0752	2.06	0.14	0.55	0.55	0.91	32	1.4×10^5	7.1	0.019
J1954 + 2923	0.43	0.0002	0.01	0.01	0.02	39	2.3×10^7	11.0	0.002
J2136 − 1606	1.23	0.16	0.14	0.14	0.24	34	7.6×10^5	6.6	0.009
J2144 − 3933	8.51	0.50	2.09	2.10	3.48	41	1.5×10^6	8.9	0.001
J2251 − 3711	12.12	13.10	12.74	12.85	21.25	34	3.1×10^4	6.0	0.014
J2310 + 6706	1.94	0.08	0.39	0.39	0.65	34	2.9×10^5	7.4	0.012

2013; Timokhin & Harding 2015; Philippov, Timokhin & Spitkovsky 2020), almost the entire region of open field lines can be considered in a vacuum approximation: $\rho_{\rm e} = 0$. Using this approximation, we constructed an exact 3D solution for longitudinal electric field $E_\parallel$ in the polar regions of a neutron star

$$E_\parallel = -\frac{1}{2}\frac{\Omega B_0 R_0}{c}\cos\chi \times$$
$$\sum_i c_i^{(0)}\lambda_i^{(0)}\left(\frac{r}{R}\right)^{-\lambda_i^{(0)}/\theta_0 - 1} J_0\left(\lambda_i^{(0)}\theta/\theta_0\right)$$
$$-\frac{1}{4}\frac{\Omega B_0 R_0}{c}\frac{R_0}{R}\sin\varphi\sin\chi \times$$
$$\sum_i c_i^{(1)}\lambda_i^{(1)}\left(\frac{r}{R}\right)^{-\lambda_i^{(1)}/\theta_0 - 1} J_1\left(\lambda_i^{(1)}\theta/\theta_0\right)$$
$$-\frac{3}{16}\left(\frac{f}{f_*}\right)^{1/2}\left(1 - \frac{f}{f_*}\right)\frac{\Omega B_0 R_0^3}{cR^2}\left(\frac{l}{R}\right)^{-1/2}\sin\varphi\sin\chi. \quad (6)$$

Here, R is the star radius, B_0 is the magnetic field at the star magnetic pole,

$$R_0 = f_*^{1/2}\left(\frac{\Omega R}{c}\right)^{1/2} \quad (7)$$

is the polar cap radius, $f_* \approx 1$ is the standard dimensionless polar cap area, and l is the distance along the magnetic field line $f =$ const. Finally, $\lambda_i^{(0,1)}$ are the zeros of the Bessel functions $J_{0,1}(x)$, and the expansion coefficients $c_i^{(0,1)}$ satisfy the conditions

$$\sum c_i^{(0)} J_0\left(\lambda_i^{(0)}x\right) = 1 - x^2 \quad (8)$$

$$\sum c_i^{(1)} J_1\left(\lambda_i^{(1)}x\right) = x - x^3. \quad (9)$$

Accordingly, the potential drop $\psi(r_m, \varphi_m)$ over the polar cap with the polar coordinates r_m, φ_m on the scale $l \sim R_0$ can be written down as

$$\psi(r_m, \varphi_m) = \frac{1}{2}\frac{\Omega B_0 R_0^2}{c}\left(1 - \frac{r_m^2}{R_0^2}\right)\cos\chi$$
$$+\frac{3}{8}\frac{\Omega B_0 R_0^2}{c}\frac{r_m}{R}\left(1 - \frac{r_m^2}{R_0^2}\right)\sin\varphi_m\sin\chi. \quad (10)$$

Knowing now the longitudinal electric field $E_\parallel$ (6), we can determine the production rate of secondary particles at sufficiently large periods P.

Note that as one can see from (6), in real dipole geometry, for non-zero inclination angles χ, the longitudinal electric field does not vanish on the scale $l \sim R_0$, which was previously assumed by Muslimov & Tsygan (1992). It decreases much more slowly, as $\propto (l/R)^{-1/2}$. This effect, however, is significant only for almost orthogonal rotators due to the additional factor R_0/R.

Next, the corrections related to the effects of general relativity were taken into account. First of all, as is well known (Beskin 1990; Muslimov & Tsygan 1992; Philippov et al. 2015, 2020), the effects of general relativity increase the electric potential (and, hence, the particle energy) as $\psi_{GR} = K_\psi \psi$, where

$$K_\psi = \left(1 - \frac{\omega}{\Omega}\right)\left(1 - \frac{r_{\rm g}}{R}\right)^{-1}. \quad (11)$$

Here, $r_{\rm g} = 2GM/c^2$ is the gravitational radius, and

$$\frac{\omega}{\Omega} = \frac{I_{\rm r} r_{\rm g}}{MR^3}, \quad (12)$$

where ω is the Lense–Thirring angular velocity (M and $I_{\rm r}$ are the neutron star mass and moment of inertia, respectively). However, to determine all the characteristics of particle production, we also need the corrections to the curvature radius of the magnetic field line $R_{\rm c}$ as well as to the polar cap radius R_0: $R_{\rm c,\,GR} = K_{\rm cur}R_{\rm c}$ and $R_{0,\,\rm GR} = K_{\rm cap}R_0$. As was shown in Paper I, they look like

$$K_{\rm cur} = 1 - \frac{1}{2}\frac{r_{\rm g}}{R}, \quad (13)$$

$$K_{\rm cap} = 1 - \frac{3}{8}\frac{r_{\rm g}}{R}. \qquad (14)$$

Finally, the magnetic field on the star surface B_0, due to a well-known correction to the magnetic flux (Ginzburg 1964), increases as $B_{0,\,\rm GR} = K_B B_0$, where

$$K_B = 1 + \frac{3}{4}\frac{r_{\rm g}}{R}. \qquad (15)$$

Note that such an increase in the magnetic field takes place if we fix its asymptotic behaviour at large distances from the neutron star. As will be shown below, it is precisely this case that is of interest.

Further, it was shown that the secondary particles generated at the smallest distance from the place of γ-quanta radiation, correspond to the γ-quantum energy, which significantly exceeds the characteristic energy of the curvature radiation $\hbar\omega_{\rm c}$, where

$$\omega_{\rm c} = \frac{3}{2}\frac{c}{R_{\rm c}}\gamma_{\rm e}^3. \qquad (16)$$

Denoting this energy as $\xi\hbar\omega_{\rm c}$, it was shown that the values of ξ are to be determined from the relation

$$\xi^{5/2}\, e^{\xi}\left(1 - \frac{55}{72}\frac{1}{\xi} + \dots\right) = \mathcal{K}, \qquad (17)$$

where

$$\mathcal{K} = \frac{4\sqrt{2}}{3\sqrt{3\pi}\,\Lambda}\frac{B_{\rm cr}}{B}\frac{R_{\rm c}}{a_{\rm B}}\gamma_{\rm e}^{-2} \approx 40\, R_{\rm c,7} B_{12}^{-1}\gamma_7^{-2}. \qquad (18)$$

Here, $B_{\rm cr} = m_{\rm e}^2c^3/e\hbar \approx 4.4\times 10^{13}$ G is the critical magnetic field, $a_{\rm B} = \hbar^2/m_{\rm e}e^2 = 5.3\times 10^{-9}$ cm is the Bohr radius, and $\Lambda = 15$–20 is the logarithmic factor: $\Lambda \approx \Lambda_0 - 3\ln\Lambda_0$, where

$$\Lambda_0 = \ln\left[\frac{e^2}{\hbar c}\frac{\omega_B R_{\rm c}}{c}\left(\frac{B_{\rm cr}}{B}\right)^2\left(\frac{m_{\rm e}c^2}{\mathcal{E}_{\rm ph}}\right)^2\right]. \qquad (19)$$

Accordingly, $R_{\rm c,\,7} = R_{\rm c}/(10^7\,{\rm cm})$, where $R_{\rm c}$ is the curvature radius of the magnetic field lines, and $\gamma_7 = \gamma_{\rm e}/10^7$.

The corresponding values of ξ are also given in Table 1. In this case, the Lorentz-factor of primary particles was determined as $\gamma_{\rm e} = e\psi/m_{\rm e}c^2$, where ψ was taken by the relation (10) for $r_m = 0.7\,R_0$. Accordingly, the curvature radius

$$R_{\rm c} = \frac{4}{3}\frac{R^2}{r_m} \qquad (20)$$

was taken for the same distance r_m. As we see, the values of ξ for the pulsars near 'the death line' turned out to be large enough. Thus, taking this correction into account is also important for the pulsars located in 'the death valley' region.

Let us finally formulate the condition for the existence of the cascade production of particles, which we will consider as the condition which determines the position of 'the death valley'. First of all, note that the beginning of the cascade (and, hence, the filling of this region with a secondary electron–positron plasma) can be initiated by the cosmic gamma background, which, as is known, leads to 10^5–10^8 primary particles per second in the polar cap region (Shukre & Radhakrishnan 1982). It is clear that for the cascade production of secondary plasma in the open magnetic field lines region, it is necessary not only to produce particles by γ-quanta propagating from the pulsar surface (this process can take place up to heights of $H\sim R$, i.e. on the scale of the diminishing of the dipole magnetic field). It is necessary that the secondary particles return to the region of a strong longitudinal electric field, accelerate, emit hard γ-quanta, which would have time to give birth to secondary particles above the surface of the neutron star.

As for the return of secondary particles to the pulsar surface from the region $H\sim R$, then, as noted previously, it can be easily explained by the slowly decreasing longitudinal field mentioned above. On the other hand, a particle moving toward the neutron star surface will be able to acquire the required energy only at a height of $H\sim R_{\rm cap}\sim 0.01R$. Accordingly, the free path-length of a γ- quantum should be of the same order. Therefore, it is the condition for the production of secondary particles above the very surface of the pulsar that should be considered as the condition for the existence of a cascade.

According to the results in Paper I, the condition for the existence of a cascade can be written as $P < P_{\rm max}$, where

$$P_{\rm max} = 0.7\,\xi^{2/15}\frac{K_\psi^{2/5}}{K_{\rm cur}^{4/15}} f_{1.6}^{3/5}\Lambda_{15}^{2/15}R_{12}^{19/15}B_{12}^{8/15}x_0^{4/15}\mathcal{P}^{2/5}\ {\rm s}. \qquad (21)$$

Here, $f_{1.6} = f_*/1.6$, $\Lambda_{15} = \Lambda/15$, $R_{12} = R/(12\,{\rm km})$, and $I_{100} = I_{\rm r}/(100\,{\rm M}_\odot{\rm km}^2)$. The choice of such a normalization for the moment of inertia $I_{\rm r}$ is due to the fact that we will further use the results obtained by Greif et al. (2020), in which $I_{\rm r}$ is presented just in this form. Finally, the last two parameters in (21), $x_0 = r_m/R_0$ and

$$\mathcal{P}(r_m,\varphi_m) = \left(\cos\chi + \frac{3}{4}x_0\frac{R_0}{R}\sin\chi\cos\varphi_m\right)\left(1 - x_0^2\right), \qquad (22)$$

determine the dependence of the ignition condition on the position on the polar cap. Unlike in Paper I, here we explicitly write down the dependencies on all possible parameters.

2.2 Two evolutionary scenarios

It is clear that expression (21) is still not enough to define 'the death line' in the P–$\dot{P}$ diagram. For doing this, we need to express the magnetic field B_0 in terms of the observed quantities. In other words, we need to specify a braking model of radio pulsars.

Below we consider two braking models. According to the most popular model based on the results of numerical simulations (Spitkovsky 2006; Kalapotharakos, Contopoulos & Kazanas 2012; Tchekhovskoy, Philippov & Spitkovsky 2016), we have

$$\dot{P}_{\rm MHD} = \frac{\pi^2}{P}\frac{B_0^2R^6}{I_{\rm r}c^3}\left(1 + \sin^2\chi\right). \qquad (23)$$

On the other hand, according to the semi-analytical model proposed by Beskin, Gurevich & Istomin (1993), for the pulsars near 'the death line', we can write down

$$\dot{P}_{\rm BGI} = \frac{\pi^2 f_*^2}{P}\frac{B_0^2R^6}{I_{\rm r}c^3}\left(\cos^2\chi + \mathcal{C}\right). \qquad (24)$$

Here,

$$\mathcal{C} = k\left(\frac{R_0}{R}\right)^{1/2} = \varepsilon P^{-1/2} \qquad (25)$$

(P is in seconds), $k\sim 1$, and ε belongs to the range between 0.005 and 0.02 (Novoselov et al. 2020). However, the last term in (24) plays a role only for orthogonal pulsars, which we do not consider here.

The corresponding magnetic fields, determined by relations (23)–(24), are also shown in Table 1 for the characteristic values $R = 12$ km, $I_{\rm r} = 100\,{\rm M}_\odot$ km^2 and $\chi = 60^\circ$. As one can see, for these parameters, the magnetic fields $B^{\rm MHD}$ practically coincide with the values given in the ATNF catalogue (Manchester et al. 2005). On the other hand, the magnetic fields for the BGI model turn out to be twice as large.

Note that since the energy losses $J_{\rm r}\Omega\dot{\Omega}$ (and, therefore, the measured value of $\dot{P}$) depend on a magnetic field at large distances from a pulsar, the magnetic field B_0 on the neutron star surface should indeed be corrected according to relation (15). As a result, due to the same dependence of $\dot{P}$ on P and B_0, we again obtain in both cases $\dot{P}_{-15} = \beta_{\rm d} P^{11/4}$ (5), where now

$$\beta_{\rm d}^{\rm MHD} = 2.1\,\xi^{-1/2} K_{\rm GR} f_{1.6}^{-9/4} \Lambda_{15}^{-1/2} R_{12}^{5/4} I_{100}^{-1} h(x_0) F^{\rm MHD}, \tag{26}$$

$$\beta_{\rm d}^{\rm BGI} = 0.8\,\xi^{-1/2} K_{\rm GR} f_{1.6}^{-17/4} \Lambda_{15}^{-1/2} R_{12}^{5/4} I_{100}^{-1} h(x_0) F^{\rm BGI}. \tag{27}$$

Here, the coefficient

$$K_{\rm GR} = \frac{K_{\rm cur}}{K_B^2 K_\psi^{3/2}}, \tag{28}$$

describes the general relativity correction. Since $K_{\rm GR} < 1$, this coefficient, together with the parameter $\xi > 1$, decreases the value of $\dot{P}$. Finally, the functions $F(x_0, \chi)$, where

$$F^{\rm MHD}(\chi) = \frac{(1 + \sin^2\chi)}{(\cos\chi + 3/4\, x_0\,(R_0/R)\, \sin\chi\, \cos\varphi_m)^{3/2}}, \tag{29}$$

$$F^{\rm BGI}(\chi) = \frac{\cos^2\chi + k(R_0/R)}{[\cos\chi + 3/4\, x_0\,(R_0/R)\, \sin\chi\, \cos\varphi_m]^{3/2}} \tag{30}$$

and

$$h(x_0) = x_0^{-1}\left(1 - x_0^2\right)^{-3/2}, \tag{31}$$

describe the dependence on the distance from the magnetic axis $x_0 = r_m/R_0$ and on the inclination angle χ.

3 'THE DEATH VALLEY'

At the beginning, let us discuss qualitatively whether an accurate allowance for all the possible corrections reduce the value of $\beta_{\rm d}$ enough to explain the entire width of 'the death valley'. First, as we see, numerical coefficients in expressions (26) and (27) turn out to be less than the initial rough estimate $\beta_{\rm d} = 4$ obtained by Cheng & Ruderman (1979), especially for the BGI model. This is due to the fact that we used the exact value of the potential drop ψ, moreover, in the case when the plasma in the region of the open field lines is completely absent.

Next, according to Table 1, the photon energy correction ξ reaches values of 7–10, so that for the pulsars located within 'the death valley', the correction factor $\xi^{-1/2}$ turns out to be of the order of 0.3. Further, the general relativistic correction $K_{\rm GR}$ (28) for the characteristic values ($M = 1.4\,{\rm M}_\odot$, $R = 12$ km, and $I_{\rm r} = 100\,{\rm M}_\odot$ km^2) gives $K_{\rm GR} \approx 0.3$. Below, we discuss this issue in more detail, taking into account all the terms, including R and $I_{\rm r}$. But already here one can conclude that the last two factors lower the value of $\beta_{\rm d}$ by an order of magnitude. Thus, this preliminary analysis is enough to conclude that the key parameter $\beta_{\rm d}$ may be significantly less than it is usually assumed.

Thus, our qualitative discussion shows that the consistent inclusion of the above corrections really allows one to significantly shift down 'the death line' in the P–$\dot{P}$ diagram. Below, we further discuss this issue, trying to understand whether all the pulsars found in 'the death valley' can be explained within the framework of our approach.

Now we proceed to a detailed study of all the quantities included in expressions (26)–(27). At first, let us discuss the question of how the parameters of a neutron star, such as their radius R, mass M and moment of inertia $I_{\rm r}$, can affect the value of the parameter $\beta_{\rm b}$. At the same time, when analysing the possible scatter in these quantities, we use the results obtained by Greif et al. (2020), where the corresponding theoretical values are presented.

Table 2 shows the values of factor $K_{\rm g}$

$$K_{\rm g} = K_{\rm GR} R_{12}^{5/4} I_{100}^{-1}, \tag{32}$$

Table 2. Tabulation of the factor $K_{\rm g}$ (32).

M (${\rm M}_\odot$)	0.5	1.0	1.5	2.0	2.5
$R = 10$ km	4.91	0.68	0.24	0.11	–
$R = 11$ km	4.78	0.90	0.30	0.13	0.07
$R = 12$ km	4.45	1.12	**0.35**	0.15	0.07
$R = 13$ km	3.81	1.06	0.41	0.16	0.08
$R = 14$ km	–	–	–	0.17	0.09

which contains complete information about the role of these parameters. As one can see, for massive neutron stars ($M \approx 2\,{\rm M}_\odot$), the reduction factor can be as small as 0.1 or even smaller. As for the tail of this distribution, the difference between the smallest values of $K_{\rm g}$ and its average value (marked in bold) is only 0.2–0.3.

Next, we note a strong dependence of $\beta_{\rm b}$ on f_* for both braking models. As was shown by Beskin, Gurevich & Istomin (1983) and confirmed recently by Tchekhovskoy et al. (2016) (see also Gralla, Lupsasca & Philippov 2017)

$$f_* \approx f_0\left(1 + 0.2\,\sin^2\chi\right), \tag{33}$$

when $f_0 = 1.4$–1.6. Therefore, for angles χ close to 90°, we have $f_* = 1.7$–2.0. As a result, for the limit value $f_* = 2$, we get a reduction factor of 0.6 for the MHD model and 0.4 for the BGI model. But also for a more realistic case $f_* = 1.8$, we have 0.75 for the MHD model and 0.6 for the BGI model. In general, as one can see, the position of 'the death line' depends very much on f_* (i.e. on the radius of the polar cap R_0). Below, we discuss this issue in greater detail.

Further, despite the low power 1/2, some decrease in the value of $\beta_{\rm d}$ can also be connected with the quantity $\Lambda = \Lambda_0 - 3\ln\Lambda_0$, where Λ_0 is given by (19). As one can see from Table 1, for most pulsars located in 'the death valley', the values of Λ are 35–40, while the normalization $\Lambda = 15$ in (26)–(27) was given for ordinary pulsars ($P = 1$ s, $\dot{P}_{-15} = 2$). As a result, this reduction factor turns out to be $\Lambda_{15}^{-1/2} \approx 0.6$.

As for the factor $h(x_0)$, taking into account the distribution of the potential ψ from the distance x_0 to the magnetic axis, it is easy to check that $h(x_0) \approx 3$ for $0.5 < x_0 < 0.6$. Therefore, in what follows, we put

$$h(x_0) \approx 3.1. \tag{34}$$

Finally, note a completely different dependence of the functions $F(\chi)$ (29)–(30) on the angle χ (they are normalized so that $F(0) = 1$). If in the MHD model, the function $F(\chi)$ increases with increasing the angle χ (and, therefore, large angles χ do not help us explain the small values of $\beta_{\rm b}$), in the BGI model, the function $F(\chi)$ decreases with increasing χ reaching a minimum at $\chi \sim 90°$. The corresponding values of $F^{\rm BGI}$ are given in Table 3 for $x_0 = 0.7$. Unfortunately, the inaccuracy in determining the coefficient k in (25) gives a significant spread in the values of $F^{\rm BGI}$. Nevertheless, it can be stated with certainty that here, too, the reducing factor can reach the values 0.3–0.4. However, in what follows, we put

$$F^{\rm BGI} = 0.7, \tag{35}$$

because this value will better fit the entire angle range χ. We emphasize once again that the minimum values F for the BGI model are achieved at large inclination angles $\chi \sim 90°$, while in the MHD model, the smallest values of F occur at angles χ close to 0°.

Fig. 2 shows 'the death lines' for the models MHD (top) and BGI (bottom). The solid lines correspond to the average value of the parameters in expressions (26)–(27) ($\xi = 9$, $\Lambda = 35$, $f_* = 1.6$, $K_{\rm g} = 0.35$, and $F = 1$), and the dashed line corresponds to their limiting

Table 3. Minimum values of the factor $F^{\rm BGI}$ (30) for $x_0 = 0.7$. The values in the parentheses show the appropriate inclination angles χ.

P(s)	0.5	1	2	4	8	16
$k = 0.2$	0.38	0.36	0.33	0.31	0.29	0.27
	(84°)	(86°)	(86°)	(87°)	(87°)	(87°)
$k = 0.5$	0.51	0.47	0.44	0.41	0.38	0.35
	(80°)	(82°)	(83°)	(84°)	(85°)	(86°)
$k = 1$	0.62	0.57	0.53	0.49	0.45	0.42
	(75°)	(80°)	(81°)	(82°)	(84°)	(84°)
$k = 2$	0.75	0.69	0.64	0.59	0.54	0.52
	(70°)	(75°)	(77°)	(80°)	(81°)	(82°)
$k = 4$	0.90	0.83	0.77	0.71	0.65	0.60
	(60°)	(65°)	(70°)	(75°)	(77°)	(80°)

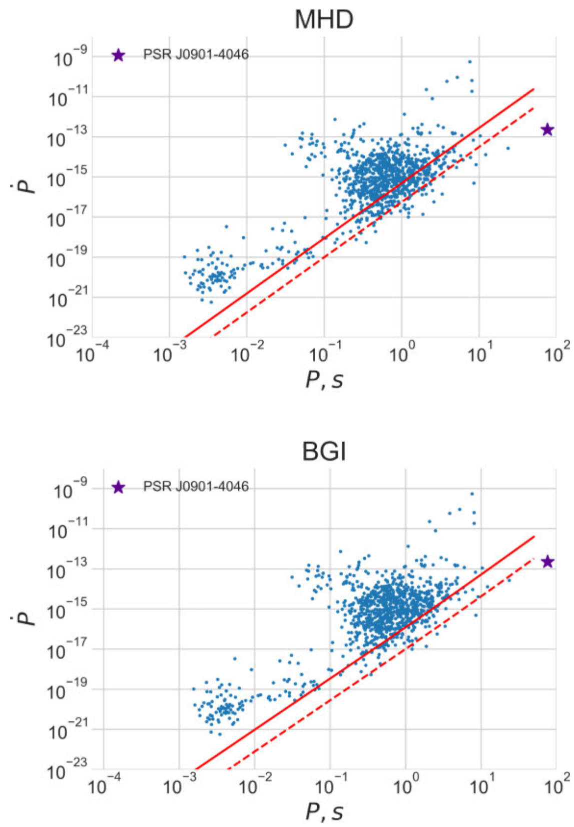

Figure 2. 'The death lines' for models MHD (top) and BGI (bottom). The solid lines correspond to the average value of the parameters in the expressions (26)–(27), and the dashed lines correspond to their limiting values.

values ($\xi = 11$, $\Lambda = 41$, $f_* = 1.9$, $K_{\rm g} = 0.07$, and $F^{\rm BGI} = 0.7$). A small break at small periods is associated with the dependence of R_0 on P. As we see, in general, both models quite well reproduce the lower boundary of 'the death valley'.

Of course, long-period pulsars ($P > 3$ s) are of special interest, especially recently discovered pulsar J0901 − 4046 ($P \approx 46$ s, Caleb et al. 2022). In particular, the question arises whether the slope of 'the death line' can be approximated by the dependence $\dot{P} = \beta_{\rm d} P^{11/4}$ considered here. In our opinion, the number of pulsars with periods $P > 3$ s located near the lower boundary of 'the death valley' is insufficient to speak of a change in its shape. On the other hand, it is useful to consider these pulsars in more detail.

Table 4 lists the data for six long-period pulsars. Theoretical values $\beta_{\rm d}^{\rm (MHD)}$ and $\beta_{\rm d}^{\rm (BGI)}$ for two models of evolution correspond to the

Table 4. Slowly rotationg pulsars ($P > 3$ s) located deep below 'the death line' ($\beta_{\rm d} < 0.02$) taken from the ATNF catalogue (Manchester et al. 2005). Theoretical values $\beta_{\rm d}$ correspond to the limiting parameters discussed in the text.

PSR	P (s)	$\dot{P}_{-15}$	$\beta_{\rm d}$	$\beta_{\rm d}^{\rm (MHD)}$	$\beta_{\rm d}^{\rm (BGI)}$
J0250 + 5854	23.53	27.16	0.003	0.013	0.002
J0418 + 5732	9.01	4.10	0.010	0.018	0.003
J1210 − 6550	4.24	0.43	0.008	0.017	0.003
J0901 − 4046	75.89	215.	0.001	0.013	0.001
J1503 + 2111	3.32	0.14	0.005	0.016	0.003
J2144 − 3933	8.51	0.50	0.001	0.014	0.002
J2251 − 3711	12.12	13.10	0.014	0.016	0.003

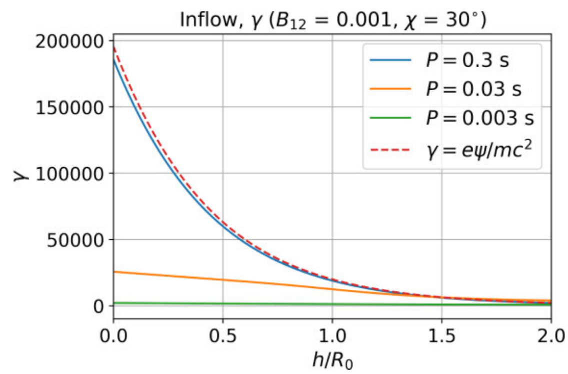

Figure 3. Lorentz factor $\gamma(h)$ of back-moving primary particles depending on the distance h from the star surface for three different periods $P = 0.003$, $P = 0.03$, and $P = 0.3$ s. The dashed line corresponds to the absence of the radiation reaction force associated with the curvature radiation.

limiting parameters discussed above. As we see, limiting BGI model ($F^{\rm BGI} = 0.27$ corresponding to almost orthogonal rotators) does not contradict the observational data. As for the difference for MHD model, we discuss this issue in Section 5.

4 'THE DEATH LINE' KNEE

Before proceeding to the analysis of the obtained results, let us discuss qualitatively one more property of 'the death line'. At the time of this writing, 3282 pulsars were already discovered (Manchester et al. 2005). This rather rich statistics clearly shows that the line limiting from below the population of pulsars on the P–$\dot{P}$ diagram has a break at $P \approx 0.3$ s (see Fig. 1). Here, we show that this break can be easily explained.

Indeed, as was shown in Paper I (see also Jones 2022), for the pulsars with small enough periods (at any way, with periods $P < 0.1$ s), the radiation reaction becomes significant, so the energy of primary particles does not reach the values dictated by the potential drop ψ (10). Clearly, this also applies to the back-moving primary particles. Fig. 3 shows the dependence of the Lorentz-factors $\gamma(h)$ of the back-moving primary particles at the distance h from the star surface for three different periods, $P = 0.003$, $P = 0.03$, and $P = 0.3$ s, for the magnetic field $B = 10^9$ G which is characteristic of millisecond pulsars. The dashed line corresponds to the case when the radiation reaction force plays no role ($\gamma = e\psi/m_{\rm e}c^2$).

As one can see, at $P < 0.3$ s, the energy of the primary particles becomes lower than previously assumed. Correspondingly, 'the death line' for these pulsars should be shifted upward compared to the dependence defined above. As a result, for the existence of cascade

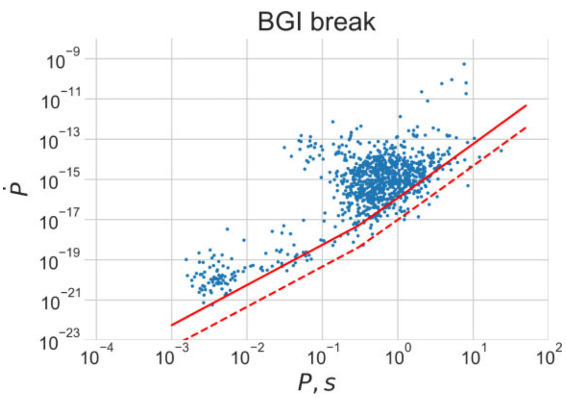

Figure 4. 'The death line' knee at period $P \approx 0.3$ s for the BGI model. At $P < 0.3$ s, the slope becomes noticeably flatter (it corresponds to proportionality $\dot{P} \propto P^2$).

particle production, the corresponding rotation periods P must be noticeably longer compared to the case in which the particle energy exactly corresponds to the accelerating potential ψ. And this, in turn, should lead to a rise in the death line in comparison with the asymptotic behaviour corresponding to the periods $P > 0.3$ s.

To evaluate this effect, one can use relation (21), in which the magnetic field B should be considered as a function of P and $\dot{P}$, and we also need to replace $\mathcal{P}$ by $k\mathcal{P}$ where the coefficient k (defined for given magnetic field $B(P, \dot{P})$, as in Fig. 3) is the decrease in particle energy due to radiation reaction

$$k = \frac{\gamma(0)}{\gamma_\psi(0)}. \qquad (36)$$

Here, $\gamma_\psi(0)$ is the Lorentz-factor of the particles with the absence of the energy losses. The resulting relation implicitly determines the dependence $\dot{P} = \dot{P}(P)$ for 'the death line'.

The corresponding break of 'the death valley' for the model BGI is shown in Fig. 4. As one can see, at $P < 0.3$ s, the slope becomes noticeably flatter (it corresponds to proportionality $\dot{P} \propto P^2$). Herewith, such 'the death valley' corresponds even better to the observations. A more detailed discussion of this issue is beyond the scope of this work.

5 DISCUSSION AND CONCLUSION

Thus, it was shown that 'the death valley' in the P–$\dot{P}$ diagram is wide enough to explain all the observed sources even for a dipole magnetic field. In this case, the best agreement takes place in the BGI model. Indeed, for the limiting values of the parameters ($\xi = 11$, $\Lambda = 41$, $f_* = 1.9$, $K_{\rm g} = 0.07$, $F^{\rm BGI} = 0.7$), we get $\beta_{\rm b} = 0.003$, which allows us to explain almost all the sources collected in Table 1. However, in our opinion, it is not worth arguing that the MHD model is inconsistent with the observational data. After all, the discrepancy here is only in factor 3 ($\beta_{\rm d} = 0.015$ for the above critical parameters, but with $F^{\rm MHD} = 1$), which can be associated with many reasons not taken into account in this work.

First of all, this difference can be related to a non-dipole magnetic field, which, as is well-known (Arons 1993; Asseo & Khechinashvili 2002; Barsukov & Tsygan 2010; Igoshev et al. 2016), leads to a decrease in the curvature radius of the magnetic field lines $R_{\rm c}$. As can be seen from relations (32) and (26)–(27), the corresponding factor $K_{\rm cur}$ enters linearly into the expression for $\beta_{\rm d}$. Hence, a decrease in the curvature radius $R_{\rm c}$ by only a few times makes it possible to explain many sources located in the lower part of 'the death valley'.

Table 5. Intermittent pulsars.

PSR	P (s)	$\dot{P}_{-15}$	$\dot{\Omega}_{\rm on}/\dot{\Omega}_{\rm off}$
J1832 + 0029	0.53	1.55	1.5
J1841 + 0500	0.91	34.7	2.5
J2310 + 6706	0.81	8.11	1.8

The second possibility is related to the size of the polar cap, the dependence on which is determined by the value f_*. A strong dependence on this parameter makes it possible to significantly reduce the value of $\beta_{\rm d}$ by a factor of three at a value of $f_* = 3$, which corresponds to an increase in the radius of the polar cap R_0 only by 20 per cent compared to the value $f_* = 1.9$ used above. Because we are unlikely to know the value of f_* with such accuracy, increasing the value of this parameter can also lower the parameter $\beta_{\rm d}$ in the MHD model.

There may be other reasons leading to a decrease in the value of $\dot{P}$. In Table 5, we collect three intermittent pulsars for which the deceleration rates both in on and off regime are known (see Beskin & Nokhrina 2007; Gurevich & Istomin 2007 for more detail; more numerous pulsars with short nullings make it impossible to determine this ratio). As one can see, in the off state, the deceleration rate of the pulsar can be 1.5–2.5 times less than in the on state. Accordingly, the long-time averaged deceleration rate $\dot{P}$ may be less than we assume.

Summing up, it was shown that 'the death valley' in the P–$\dot{P}$ diagram is wide enough to explain all the observed sources even for a dipole magnetic field. In this case, the best agreement takes place in the BGI model, although MHD model, taking into account quite reasonable additional assumptions, also does not contradict the observations. This once again proves that from the very beginning (i.e. from the works of Sturrock 1971; Ruderman & Sutherland 1975) we correctly understood the nature of the activity of radio pulsars.

ACKNOWLEDGEMENTS

The authors thank YNI and AAP for their useful discussions. This work was partially supported by Russian Foundation for Basic Research (RFBR), grant no. 20-02-00469.

DATA AVAILABILITY

The data underlying this work will be shared on reasonable request to the corresponding author.

REFERENCES

Arendt P. N., Eilek J. A., 2002, ApJ, 581, 451
Arons J., 1982, ApJ, 254, 713
Arons J., 1993, ApJ, 408, 160
Asseo E., Khechinashvili D., 2002, MNRAS, 334, 743
Barsukov D. P., Tsygan A. I., 2010, MNRAS, 410, 1077
Barsukov D. P., Kantor E. M., Tsygan A. I., 2007, Astron. Rep., 51, 469
Beskin V. S., 1990, Sov. Astron. Lett., 16, 286
Beskin V. S., Litvinov P. E., 2022, MNRAS, 510, 2572
Beskin V. S., Nokhrina E. E., 2007, Ap&SS, 308, 569
Beskin V. S., Gurevich A. V., Istomin I. N., 1983, Sov. Phys. J. Exp. Theor. Phys., 58, 235
Beskin V. S., Gurevich A. V., Istomin Y. N., 1993, Physics of the Pulsar Magnetosphere. Cambridge Univ. Press, Cambridge
Bilous A. V. et al., 2019, ApJ, 887, L23
Blandford R. D., Scharlemann E. T., 1976, MNRAS, 174, 59
Caleb M. et al., 2022, Nat. Astron., 6, 828
Cerutti B., Philippov A. A., Spitkovsky A., 2016, MNRAS, 457, 2401

Chen K., Ruderman M., 1993, ApJ, 402, 264
Cheng A. F., Ruderman M. A., 1979, ApJ, 229, 348
Daugherty J. K., Harding A. K., 1982, ApJ, 252, 337
Faucher-Giguére C.-A., Kaspi V. M., 2006, ApJ, 643, 2401
Ginzburg V. L., 1964, Sov. Phys. Doklady, 9, 329
Gonthier P. L., Ouellette M. S., Berrier J., O'Brien S., Harding A. K., 2002, ApJ, 565, 482
Gralla S. E., Lupsasca A., Philippov A., 2017, ApJ, 851, 137
Greif S. K., Hebeler K., Lattimer J. M., Pethick C. J., Schwenk A., 2020, ApJ, 901, 155
Gurevich A. V., Istomin I. N., 1985, Sov. Phys. J. Exp. Theor. Phys., 62, 1
Gurevich A. V., Istomin Y. N., 2007, MNRAS, 377, 1663
Hibschman J. A., Arons J., 2001, ApJ, 546, 382
Igoshev A. P., Elfritz J. G., Popov S. B., 2016, MNRAS, 462, 3689
Istomin Y. N., Sobyanin D. N., 2007, Astron. Lett., 33, 660
Janssen G. H., van Leeuwen J., 2004, A&A, 425, 255
Jones P. B., 2022, MNRAS, 510, 34
Kalapotharakos C., Contopoulos I., Kazanas D., 2012, MNRAS, 420, 2793
Konar S., Deka U., 2019, J. Astrophys. Astron., 40, 42
Kou F. F., Tong H., 2015, MNRAS, 450, 1990
Lorimer D. R., Kramer M., 2012, Handbook of Pulsar Astronomy. Cambridge Univ. Press, Cambridge
Lyne A., Graham-Smith F., 2012, Pulsar Astronomy. Cambridge Univ. Press, Cambridge
Manchester R. N., Hobbs G. B., Teoh A., Hobbs M., 2005, ApJ, 129, 1993
Medin Z., Lai D., 2010, MNRAS, 406, 1379
Mitra D., Rankin J. M., 2008, MNRAS, 385, 606
Muslimov A. G., Tsygan A. I., 1992, MNRAS, 255, 61
Novoselov E. M., Beskin V. S., Galishnikova A. K., Rashkovetskyi M. M., Biryukov A. V., 2020, MNRAS, 494, 3899
Philippov A. A., Spitkovsky A., Cerutti B., 2015, ApJ, 801, L19
Philippov A., Timokhin A., Spitkovsky A., 2020, Phys. Rev. Lett., 124, 245101
Riley T. E. et al., 2019, ApJ, 887, L21
Ruderman M. A., Sutherland P. G., 1975, ApJ, 196, 51
Shukre C. S., Radhakrishnan V., 1982, ApJ, 258, 121
Spitkovsky A., 2006, ApJ, 648, L51
Sturrock P., 1971, ApJ, 164, 529
Tchekhovskoy A., Philippov A., Spitkovsky A., 2016, MNRAS, 457, 3384
Timokhin A. N., 2010, MNRAS, 408, L41
Timokhin A. N., Arons J., 2013, MNRAS, 429, 20
Timokhin A. N., Harding A. K., 2015, ApJ, 810, 144
Usov V. V., Melrose D. B., 1995, Aust. J. Phys., 48, 571
van Leeuwen A. G. J., Stappers B. W., Ramachandran R., Rankin J. M., 2003, A&A, 399, 223
Weltevrede P., Edwards R. T., Stappers B. W., 2006, Chin. J. Astron. Astrophys. Suppl., 6, 13
Weltevrede P., Stappers B. W., Edwards R. T., 2007, A&A, 469, 607
Zhang B., Harding A. K., Muslimov A. G., 2000, ApJ, 531, L135

This paper has been typeset from a TEX/LATEX file prepared by the author.